Eur. Phys. J. D **12**, 161–169 (2000)

THE EUROPEAN PHYSICAL JOURNAL D

EDP Sciences

Modelling gold clusters with an empirical many-body potential

N.T. Wilson and R.L. Johnston[a]

School of Chemistry, University of Birmingham, Edgbaston, Birmingham B15 2TT, UK

Received 30 September 1999 and Received in final form 23 March 2000

Abstract. Molecular Dynamics Simulated Annealing has been used to probe the structure of small Au clusters consisting of between 2 and 40 atoms. The interatomic interactions within these clusters are described using an empirical Murrell-Mottram many-body potential energy function. Four distinct structural motifs are present in the structures of the predicted global minima, based on octahedra, decahedra, icosahedra and hexagonal prisms.

PACS. 61.46.+w Clusters, nanoparticles, and nanocrystalline materials – 36.40.-c Atomic and molecular clusters

1 Introduction

Clusters form an important link between isolated atoms and molecules at one extreme and bulk solids at the other. This central role of clusters makes their study of particular interest, with some specific areas of study being [1]: the evolution of properties such as potential energy, melting point and metallic behaviour as cluster size increases [2]; finite-size effects due to the non-periodic nature of clusters; the high proportion of atoms on the surface of a cluster leading to significant analogues of processes observed in surface science.

The fabrication of Au nanoparticles using thiolate ligands to produce colloidal solutions [3–7] has given fresh impetus to this field. These passivated clusters are relatively stable and can be easily manipulated, allowing easier experimental observations and this has lead to the application of these methods to different metals and also the use of multifunctional ligating agents such as dithiolates and bio-organic linking agents. These techniques could be used to create nanocrystalline arrays of passivated clusters which may have great technological importance in the fabrication of nanoscale devices.

Before one can study these passivated nanoparticles one must examine the properties of the bare (unpassivated) clusters. This study will focus on the structure and stability of small gold clusters which have been predicted by Molecular Dynamics Simulated Annealing (MDSA) techniques and an empirical many-body potential. Empirical potentials are important in this field due to the computational expense involved in performing *ab initio* calculations on clusters of such a heavy atom. Searching the potential energy hypersurface thoroughly using *ab initio* methods is presently computationally infeasible for more than a few atoms and therefore the information provided by empirical potentials on the nature of the potential energy surface could also be used to provide candidate structures for *ab initio* minimisations.

[a] e-mail: roy@tc.bham.ac.uk

2 Methodology

2.1 The Murrell-Mottram potential

The interactions between Au atoms are modelled by a Murrell-Mottram (MM) potential [8,9]. This potential is based on a many-body expansion of the potential energy truncated at the three body level

$$V = \sum_{i}^{N-1}\sum_{j>i}^{N} V_{ij}^{(2)} + \sum_{i}^{N-2}\sum_{j>i}^{N-1}\sum_{k>j}^{N} V_{ijk}^{(3)}. \qquad (1)$$

The effective two body term is a Rydberg energy function

$$V_{ij}^{(2)} = -D\left[(1 + a_2\rho_{ij})\,\mathrm{e}^{-a_2\rho_{ij}}\right] \qquad (2)$$

where

$$\rho_{ij} = \frac{r_{ij} - r_\mathrm{e}}{r_\mathrm{e}}\,. \qquad (3)$$

D is an energy scaling parameter which determines the well-depth, r_e gives the equilibrium pair separation and a_2 determines the hardness of the interaction.

The effective three body term is a damped polynomial in the reduced interatomic separations: ρ_{ij}, ρ_{jk} and ρ_{ki} (as defined in Eq. (3)). This term must be symmetrical with respect to the interchange of like atoms and therefore the polynomial is not a simple function of the interatomic separations but is an expansion in terms of symmetry coordinates, Q_i, defined as

$$\begin{pmatrix} Q_1 \\ Q_2 \\ Q_3 \end{pmatrix} = \begin{pmatrix} \sqrt{1/3} & \sqrt{1/3} & \sqrt{1/3} \\ 0 & \sqrt{1/2} & -\sqrt{1/2} \\ \sqrt{2/3} & -\sqrt{1/6} & -\sqrt{1/6} \end{pmatrix} \begin{pmatrix} \rho_{ij} \\ \rho_{jk} \\ \rho_{ki} \end{pmatrix}. \qquad (4)$$

Table 1. MM potential parameters for Au [10].

parameter	fitted value
a_2	9.0
a_3	10.0
D /eV	1.0912
r_e /Å	2.7725
c_0	0.2794
c_1	−0.2770
c_2	5.3532
c_3	−2.4844
c_4	5.4158
c_5	−11.0954
c_6	5.9364

The effective three body term is thus given by

$$V_{ijk}^{(3)} = DP(Q_1, Q_2, Q_3)\, F(a_3, Q_1) \tag{5}$$

where D is the same energy scaling parameter as in the pair potential, $P(Q_1, Q_2, Q_3)$ is the polynomial in the symmetry coordinates and $F(a_3, Q_1)$ is a damping function which constrains the effective three body term to approach zero as Q_1 becomes large.

The Q_i are irreducible representations of the permutation group S_3. All totally symmetric polynomials can be written as sums and products of the following three functions: Q_1, $Q_2^2 + Q_3^2$ and $Q_3^3 - 3Q_3Q_2^2$.

The polynomial term in $V^{(3)}$ can be cubic or quartic. In this study a cubic potential, given by

$$P(Q_1, Q_2, Q_3) = c_0 + c_1Q_1 + c_2Q_1^2 + c_3(Q_2^2 + Q_3^2) + c_4Q_1^3 + c_5Q_1(Q_2^2 + Q_3^2) + c_6(Q_3^3 - 3Q_3Q_2^2), \tag{6}$$

was adopted.

The damping function is of the form

$$F(a_3, Q_1) = \mathrm{sech}(a_3Q_1). \tag{7}$$

The MM potential has been applied to a wide range of elemental systems including alkali metals, alkaline earth metals, Group 13 metals, Group 14 semiconductors, transition metals, coinage metals and the lanthanides [9]. The MM potential is parameterised to bulk experimental properties such as lattice and vacancy formation energies, lattice spacing, elastic constants, and phonon frequencies. The MM potential for Au used is this study was parameterised by Cox *et al.* and has been used to model the reconstructions of Au surfaces [10]. The fitted parameters for this potential are given in Table 1. Though studies of coinage metal surfaces were previously carried out using MM potentials with quartic three-body terms [11,12], the re-optimised potential of Cox *et al.* with cubic three-body terms, as used in this study, has been found to be more accurate for calculating surface energies and surface reconstructions [10] which is an important consideration as clusters have a high ratio of surface to bulk atoms.

2.2 Cluster energetics

The (average) binding energy (per atom), E_b, of an N atom cluster is defined as

$$E_b(N) = -\left(\frac{V}{N}\right) \tag{8}$$

$$= -\frac{1}{N}\left(\sum_{i}^{N-1}\sum_{j>i}^{N} V_{ij}^{(2)} + \sum_{i}^{N-2}\sum_{j>i}^{N-1}\sum_{k>j}^{N} V_{ijk}^{(3)}\right) \tag{9}$$

and gives a quantity which can be compared between clusters of different sizes. The binding energy can be partitioned into contributions from the effective two body and three body term thus

$$E_b(N) = E_b^{(2)}(N) + E_b^{(3)}(N) \tag{10}$$

$$E_b^{(2)}(N) = -\frac{1}{N}\left(\sum_{i=1}^{N-1}\sum_{j>i}^{N} V_{ij}^{(2)}\right) \tag{11}$$

$$E_b^{(3)}(N) = -\frac{1}{N}\left(\sum_{i=1}^{N-2}\sum_{j>i}^{N-1}\sum_{k>j}^{N} V_{ijk}^{(3)}\right). \tag{12}$$

The second difference in the binding energy is defined by

$$\Delta_2 E_b(N) = 2E_b(N) - E_b(N-1) - E_b(N+1) \tag{13}$$

and gives an indication of the stability of a cluster with respect to disproportionation [13].

The difference in E_b between the predicted global minimum, $E_b(N,1)$, and the next best (*i.e.* the next lowest energy) minimum found, $E_b(N,2)$, defined as $\Delta E_b(N)$, is given by

$$\Delta E_b(N) = E_b(N,1) - E_b(N,2). \tag{14}$$

2.3 Computational details

The MDSA protocol involves the slow quenching of a cluster from a high temperature, usually liquid-like, configuration into a low energy conformation whilst probing the thermally accessible regions of phase space [14]. At high temperatures, the system is able to occupy high energy regions of conformational space and to pass over high energy barriers. As the temperature falls, the lower energy states become more probable, according to the Boltzmann distribution. At absolute zero the system should occupy the lowest energy state (*i.e.* the global minimum), though to guarantee that the global minimum is reached would require an infinite number of temperature steps, at each of which the system would have to come to equilibrium [15]. Since infinitely slow cooling is not possible in practice, more than one trajectory is followed for each cluster size.

The MDSA study was performed using the CLUSPRO [16] suite of programs and has the following general features.

Initial Cluster Geometry: this was generated by placing N atoms at random positions (employing the random number generator from Numerical Recipes [17]) within a sphere of radius $\propto N^{1/3}$ whilst ensuring no two atoms have a separation of less than $0.7\,r_e$ and all atoms have at least one neighbouring atom within a radius of $1.3\,r_e$. These conditions produce a compact pseudo-spherical initial geometry.

Equilibration: the initial configuration is equilibrated at a chosen initial temperature for a simulation time of 10 ps with a timestep of 10^{-15} s. The temperature is defined as $T = 2\langle E_k\rangle/(3N - N_c)k$ [14], where $\langle E_k\rangle$ is the time averaged kinetic energy and N_c is 5 if $N = 2$ and 6 otherwise.

Annealing: the cluster is slowly cooled over a simulation time of between 100 ps and 900 ps by periodically rescaling the velocities to reproduce a continually decreasing temperature.

Quenching: fifty times during the annealing process the MD is stopped and the current basin of attraction of the cluster is determined by performing a local minimisation (employing the L–BFGS quasi-Newton minimisation routine [18]). The cluster is then returned to its previous configuration on the MD trajectory and the annealing process continues.

Minima storage: the ten best minima found during the quenching process and the final annealed geometry were stored in order to build a database of low energy conformations for each nuclearity.

Fifty annealing runs were performed for each cluster nuclearity for each of five initial temperatures (in the range 1250–1750 K) with different cooling rates governed by the initial temperature and simulation time of the annealing step (100–900 ps as outlined above). This procedure has proved adequate to determine with reasonable certainty the global minima within this size range.

3 Results and discussion

Figure 1 shows the progress of a single MDSA run for a 20 atom cluster annealed from 1500 K with a simulation time of 100 ps. The solid line is the instantaneous potential energy of the cluster as it is annealed and the open circles are the potential energies of the minima found during the quenching steps. The cluster hops in and out of the basin of attraction of the global minimum before finally annealing into that configuration.

The binding energies (defined in Eq. (8)), structures and symmetries of the predicted global minima for Au_{2-20} are listed in Table 2 and the binding energies and symmetries for Au_{21-40} are given in Table 3. Figure 2 shows the structures for Au_{2-40}. Following Northby *et al.* [19] and Lee and Stein [20], Figure 3 shows the binding energies for Au_{2-40} relative to a best fit cubic polynomial in $N^{-1/3}$

$$E_{\rm fit}(N)/{\rm eV} = 3.645 - 1.892N^{-1/3} - 3.839N^{-2/3} + 1.614N^{-1}. \quad (15)$$

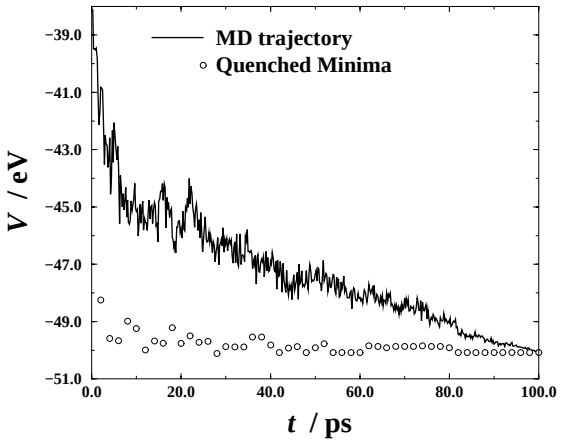

Fig. 1. Evolution of instantaneous potential energy (solid line) during an MD annealing simulation for Au_{20}. The circles indicate the local (or global) minima obtained by quenching the potential energy.

Table 2. The structures and binding energies of the global minima for Au_{2-20}.

N	structure	symmetry	E_b/eV
2	dimer	$D_{\infty h}$	0.545586
3	trimer	D_{3h}	0.989788
4	tetrahedron	T_d	1.333830
5	trigonal bipyramid	D_{3h}	1.538039
6	octahedron	O_h	1.746333
7	pentagonal bipyramid	D_{5h}	1.841928
8	dodecahedron	D_{2d}	1.955007
9	tricapped trigonal prism	D_{3h}	2.040154
10	bicapped square antiprism	D_{4d}	2.104379
11	octadecahedron	C_{2v}	2.153433
12	uncentred icosahedron	I_h	2.203745
13	centred icosahedron	I_h	2.271417
14	bicapped hexagonal antiprism	D_{6d}	2.309511
15	capped decahedron	C_{2v}	2.343431
16	capped decahedron	C_s	2.389115
17	capped decahedron	D_{4d}	2.435400
18	capped decahedron	C_{4v}	2.464642
19	capped decahedron	D_{4d}	2.490743
20	capped decahedron	C_{2v}	2.505752

Positive values of $E_b(N) - E_{\rm fit}(N)$ correspond to structures which have a greater than average binding energy and it can be seen that Au_{6-10}, Au_{16-20} and Au_{34-40} are all regions where the predicted global minima have higher than average binding energy.

A plot of the second difference in binding energy (as defined in Eq. (13)) is shown in Figure 4. A peak in this plot corresponds to a structure which is stable with respect to its neighbouring nuclearities and such plots are

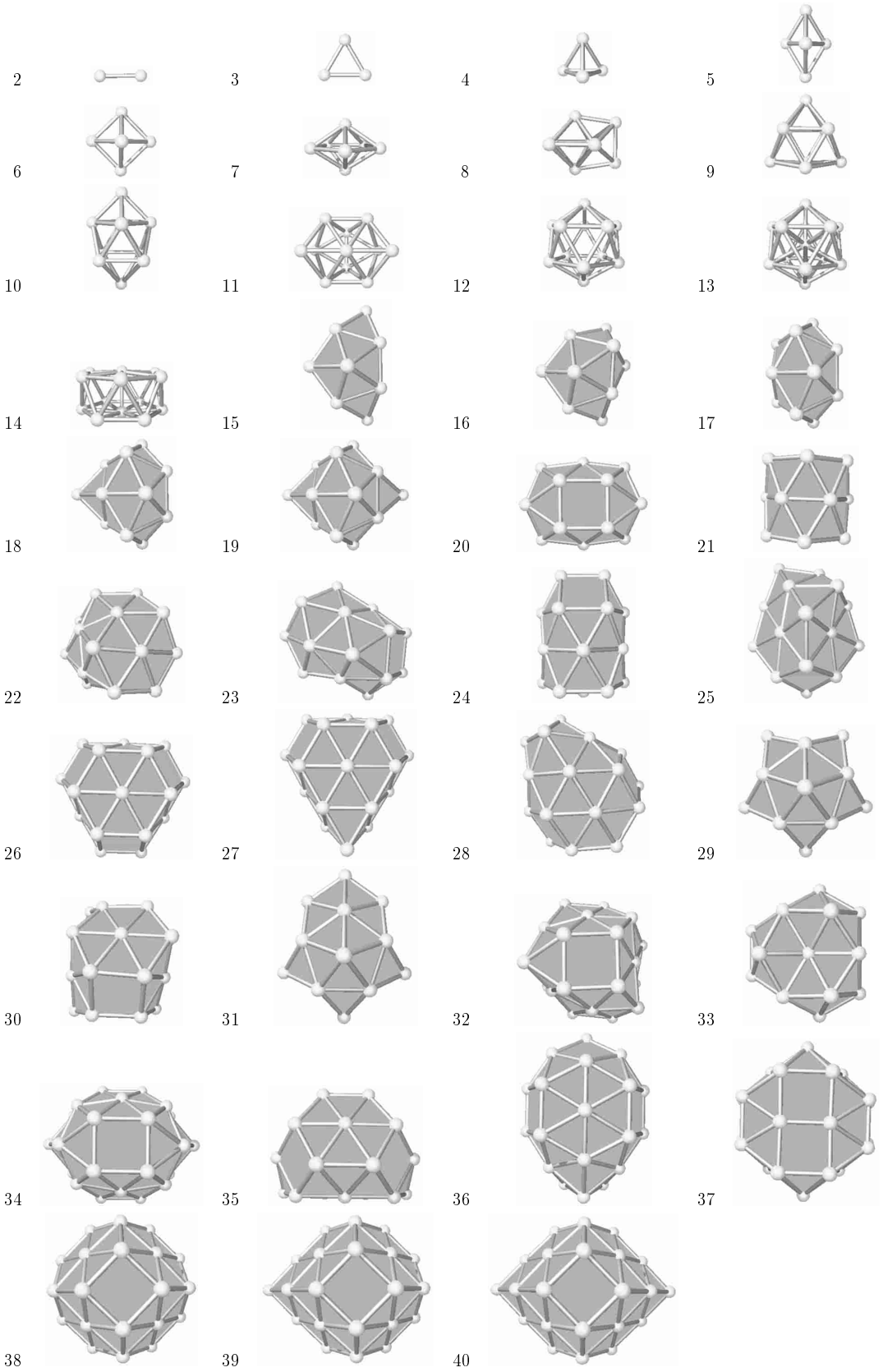

Fig. 2. The structures of the predicted global minima for Au_{2-40} (structures after Au_{14} have their surfaces shaded for clarity).

Table 3. The symmetries and binding energies of the global minima for Au_{21-40}.

N	symmetry	E_b/eV
21	C_{2v}	2.537888
22	C_2	2.551077
23	C_1	2.563818
24	C_{3v}	2.586055
25	C_1	2.603524
26	D_{3h}	2.625183
27	C_s	2.638021
28	C_s	2.652710
29	D_{5h}	2.672138
30	C_1	2.686964
31	C_{2v}	2.700586
32	C_2	2.716558
33	C_s	2.729413
34	C_{2v}	2.744327
35	C_{2v}	2.754212
36	C_s	2.768073
37	C_{2v}	2.777858
38	O_h	2.803364
39	C_{4v}	2.807726
40	D_{4h}	2.811867

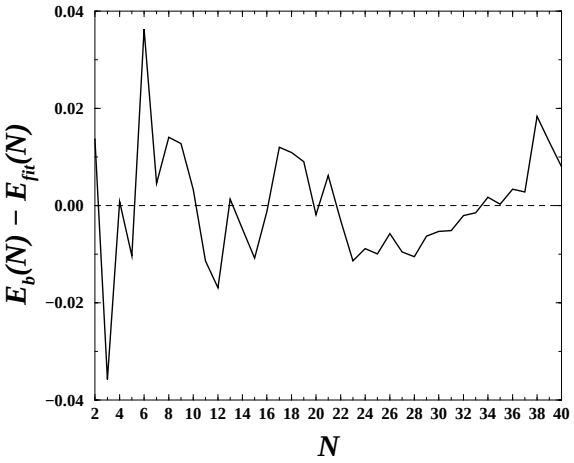

Fig. 3. Fluctuations in the binding energy (E_b) of Au_{2-40} relative to the size-dependent average energy (E_{fit}) defined in equation (15).

often used to rationalise intensities in mass spectral data [1]. The different structural motifs in this size range are shown by the symbols on the graph. The terms "octahedral", "icosahedral", "decahedral" and "hexagonal prism" denote that the geometry for that nuclearity is based on that structural motif but may have capping atoms, reconstructions or distortions. Neighbouring hexagonal planes in the "hexagonal prisms" are actually rotated with respect to each other (*i.e.* they are strictly anti-prismatic

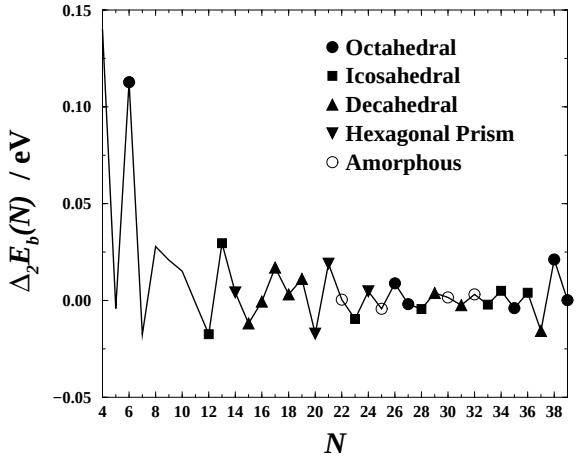

Fig. 4. Second difference in binding energy (as defined in Eq. (13)) of Au_{4-39}.

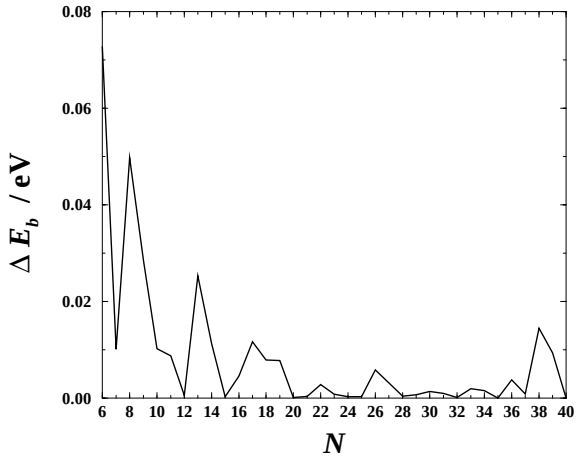

Fig. 5. Difference in binding energy (as defined in Eq. (14)) between the two lowest energy minima of Au_{6-40}.

locally), but the shorter name has been used to encompass multi- as well as 2-layer clusters. Finally, the term "amorphous" refers to structures (usually with C_1 symmetry) which do not correspond to any of the above structural motifs. It should be noted that no single structural motif dominates the predicted global minima over this size range, as opposed to observations in the Lennard-Jones system where the icosahedral structural motif dominates [21].

The pronounced peak in the second difference for Au_6 shows that the octahedron is a very stable species. The highly symmetrical icosahedral Au_{13} structure and truncated octahedral Au_{38} structures also correspond to pronounced peaks. Au_{21} which is a reconstructed triple layer hexagonal prism and Au_{17} which has D_{4d} symmetry with a structure based on a distorted tetra-capped decahedron, also show pronounced peaks.

The differences in E_b between the predicted global minimum and the next best minimum found, defined as $\Delta E_b(N)$ in equation (14), are plotted against N in Figure 5. A large value of $\Delta E_b(N)$ correlates to a nuclearity for which the predicted global minimum is much more stable than all other isomers. Figure 5 has many similarities

Table 4. Comparison of *ab initio* and MM structures for Au_2.

	D_e /eV	R /Å
expt.	2.3	2.472
MM	1.09	2.772
Ref. [22]	1.87	2.56
Ref. [23]–MCSCF	1.11	2.69
Ref. [23]–CI	1.58	2.65
Ref. [24]	1.9	2.547

Table 5. Comparison of *ab initio* and MM structures for Au_3.

		E_b /eV	R /Å	θ /deg
MM	D_{3h}	0.99	2.780	60.0
Ref. [22]	C_{2v}	1.18	2.657	66.4
Ref. [24]	C_{2v}	0.93	2.642	69.4

to the plot of second difference in binding energy (Fig. 4), with large values of $\Delta E_b(N)$ for $N = 6$, 8, 13, 17, 26 and 38. The only significant peak in the second difference plot which does not correspond to a large value of $\Delta E_b(N)$ occurs for Au_{21}, for which the global minimum is a hexagonal prism which has undergone a 4 atom square-diamond reconstruction. For this nuclearity, the unreconstructed structure (which is the second most stable minimum) is very close in energy to the reconstructed structure, leading to a small value of $\Delta E_b(N)$.

In the following sections the predicted global minima for Au_{2-40} are examined more closely and compared with the results of previous calculations.

3.1 Au_{2-11}

Ab initio calculations have been performed on the Au dimer using relativistic effective core potentials [22,23], full geometry optimisation has been performed within the DFT framework on Au_{2-4} [24] and symmetry constrained DFT calculations have been performed on Au clusters with up to 147 atoms [25]. For Au_2 the MM potential overestimates the experimental bond length and underestimates the experimental dissociation energy as can be seen in Table 4. This is due to the transfer of a potential parameterised to bulk properties to a regime where finite size effects are obviously critically important. It is important to note, however, that the 2- and 3-body components of the MM potential are actually effective 2- and 3-body energies. They are fitted to the bulk where many-body (greater than 3-body) effects are present. Truncating the potential at the 3-body level means that higher order terms are subsumed into these effective 2- and 3-body terms.

For gold clusters, Jahn-Teller effects are important for clusters of more than two atoms. Results from the above *ab initio* calculations for Au_3 are summarised in Table 5. The MM potential predicts a similar binding energy but does not recreate the C_{2v} symmetry of the *ab initio* minimum.

Table 6. Comparison of *ab initio* and MM structures for Au_4.

		E_b /eV	R /Å
MM	T_d	1.334	2.7930
Ref. [24]	C_{2v}	1.239	2.761, 2.608, 2.560

Table 7. Comparison of *ab initio* and MM structures for Au_6.

		E_b /eV	R /Å
MM	O_h	1.75	2.79
Ref. [25]–GGA	O_h	1.55	2.78
Ref. [25]–LDA	O_h	2.26	2.70

The DFT calculations mentioned above for Au_4 are compared to those from this study in Table 6. They predict a C_{2v} symmetry as the global minimum which consists of an isosceles trimeric unit with an atom bonded to the apex whereas the MM potential predicts T_d symmetry, the structure which would be predicted from purely geometrical considerations. The trigonal bipyramid is predicted to be the global minimum for Au_5.

Symmetry constrained DFT calculations on Au_6 [25] are compared to those from this study in Table 7. The binding energy predicted by the MM potential lies between the LDA value, which overestimates the bulk binding energy, and the GGA value, which underestimates the bulk binding energy.

Au_7 has a pentagonal bipyramidal structure and Au_8 has a dodecahedral structure formed by capping two adjacent octahedral faces. Au_9 is a tricapped trigonal prism and Au_{10} is a square antiprism with capping atoms on the two square faces. Au_{11} has an octadecahedral structure which can be formed by removing two adjacent vertices of a centred icosahedron and translating the central atom towards the missing edge.

The global minima predicted (using the MM potential) for Au_{5-11} are isostructural with the *closo*-boranes $[B_NH_N]^{2-}$. The predicted global minima for Au_{3-8} and Au_{11} are identical to those obtained for gold clusters by Doye and Wales using a Sutton-Chen potential [26].

3.2 Au_{12-13}

The predicted global minimum for Au_{12} with the MM potential is the uncentred icosahedron. Previous studies have shown that the C_{5v} structure, consisting of a centred icosahedron with a vertex missing, is usually preferred for 12 atom metal clusters (though Doye and Wales predict a lower symmetry structure for Au_{12} itself [26]). These two structures, and the 13 atom centred icosahedron from which they are derived, are shown in Figure 6. The binding energies have been partitioned into the effective two and three body contributions (as defined in Eqs. (10–12)) and this information is given in Table 8. The C_{5v} structure

Fig. 6. Structures of the 13 atom centred icosahedron and its 12 atom derivatives.

Table 8. Binding energies (and 2- and 3-body components) of the 13 atom centred icosahedron and its 12 atom derivatives.

N		$E_b^{(2)}$ /eV	$E_b^{(3)}$ /eV	E_b /eV
12	C_{5v}	2.79	−0.59	2.20
12	I_h	3.20	−1.02	2.18
13	I_h	3.45	−1.18	2.27

Table 9. Comparison of DFT [25] and MM energies for Au_{13}. The O_h symmetry refers to the cuboctahedral geometry.

	E_b /eV		
	MM	LDA	GGA
O_h	2.24	2.84	1.95
I_h	2.27	2.79	1.88

for Au_{12} has a large attractive effective two body contribution to the binding energy, denoting stronger nearest-neighbour bonding in this compact structure relative to the uncentred I_h structure for Au_{12}. The radial distance in an icosahedron is approximately 5% shorter than the surface distance and as there are 30 surface bonds compared to 12 radial bonds the radial bonds are compressed to maximise the binding in the cluster [27]. The compression in the C_{5v} structure leads to a large repulsive effective three body contribution to the binding energy which destabilises this structure relative to the uncentred I_h structure which has no compressed radial bonds. Although the MM potential is a model potential, it would be interesting to determine if such hollow structures may in fact be found experimentally for clusters of gold or other metals.

Symmetry constrained DFT calculations have been performed by Häberlen *et al.* [25] on cuboctahedral and octahedral gold clusters with up to 147 atoms. The cuboctahedron is more stable than the icosahedron for Au_{13} within both the LDA and the GGA approximations. The binding energies for these minima are compared to those predicted by the MM potential in Table 9. Although the energies calculated with the MM potential lie between the LDA and GGA values, the MM potential prefers the icosahedron over the cuboctahedron. Jahn-Teller distortions which have not been considered here may lower the symmetries of these structures.

3.3 Reconstructions

Au surfaces are known to undergo structural reconstructions and the potential used in this study has been shown to model these reconstructions well [10]. As clusters have a high proportion of atoms on their surface, it is not surprising that some of the minima found in this study also undergo reconstructions or are distorted from regular structures, notably Au_{15-19} which are distorted capped decahedra and Au_{21} which has a 4 atom square-diamond reconstruction on its surface. Capped decahedral structures (both distorted and undistorted) have been observed for a variety of metals bound by MM potentials [28,29]. However, with the exception of Pt, all other metals that we have investigated with MM potentials have the D_{5h} symmetry double icosahedron as their global minimum for $N = 19$ [29]. The double icosahedron is also predicted to be the global minimum for 19 atom Lennard-Jones and Morse potentials [26,30]. Finally, it is interesting to note that Au and Pt were also found generally to have different global minima from their lighter congeners in the Sutton-Chen study by Doye and Wales [26].

3.4 Comparison with other empirical potentials

Global minima for the Lennard-Jones potential [21], the Morse potential (with range exponents ranging from 3 to 14) [30], and a Sutton-Chen potential parameterised for Au [26] are all available from the Cambridge Cluster Database [31]. These structures were compared with those obtained using the MM potential to establish at which nuclearities the global minima predicted by these different potentials are equivalent. The commonalities are outlined in Table 10 along with those obtained using the many-body Gupta potential [32–37]. For Au_{2-5} the MM potential only has one minimum and the other potentials considered also have the same structures as their global minima. The predicted global minima for Au_{6-8} are also similar for all the potentials due to the small number of viable minima at these small nuclearities. The 13 atom icosahedron is common to all potentials due to its highly symmetrical nature and Au_{38} is frequently found to be particularly stable and also has a highly symmetrical truncated octahedral motif. For the Sutton-Chen potential the 14 and 21 atom clusters are also hexagonal prismatic in nature except that there is no rearrangement for the 21 atom cluster and the central atoms are translated along the prism axis. The 15–20 atom clusters are decahedral in nature, as observed in this study, although the arrangement of capping atoms and distortions are different. The 37 atom Sutton-Chen cluster is also based on a decahedron, as observed in this study. It is apparent from these results that the MM potential energy surface has certain regions of similarity to the other potentials but it also has regions which are unique to this potential.

An Embedded Atom Model (EAM) has been applied to Au clusters by Landman *et al.* [5–7] and this also predicts a truncated octahedral motif for Au_{38}. The n-body Gupta potential, adopted by Garzòn and Jellinek

Table 10. Nuclearities at which various potentials predict a similar Global Minimum to the MM potential (LJ denotes Lennard-Jones, Morse (3, 6, 10, 14) refers to a Morse potential with the corresponding range parameter, SC denotes the Sutton-Chen 10–8 potential and Gupta denotes the Gupta potential as implemented in references [32–37]. Only nuclearities at which a similar global minimum is found are shown and comparisons are possible for nuclearities of 6 to 40 for LJ, Morse and SC and for nuclearities of 6, 7, 12, 13, 14, 19 and 38 for the Gupta potential.

N	potentials in common with MM			
6	LJ	Morse (3, 6, 10, 14)	SC	Gupta
7	LJ	Morse (3, 6, 10, 14)	SC	Gupta
8		Morse (3, 6, 10, 14)	SC	
9		Morse (3)		
11	LJ	Morse (3)		
13	LJ	Morse (3, 6, 10, 14)	SC	Gupta
14			SC	Gupta
16			SC	
31		Morse (14)		
37			SC	
38	LJ	Morse (10, 14)	SC	
39		Morse (10, 14)	SC	
40		Morse (10, 14)	SC	

[32,33], Garzòn *et al.* [34–36], Sawada and Sugano [37], and Ercolessi, Andreoni and Tosatti [38], finds a disordered structure to be slightly more stable than the truncated octahedron for Au_{38}. The Gupta potential also predicts that, in common with this study, the octahedron is the global minimum for Au_6, the pentagonal bipyramid is the global minimum for Au_7 and that a hexagonal anti-prismatic structure is the global minimum for Au_{14}, except that the Gupta potential predicts the central two atoms are translated along the axis of the prism, as for the Sutton-Chen potential. The Gupta potential also predicts a structure based on a decahedron for Au_{19}, except that the arrangement of the capping atoms is different.

4 Conclusions

Four distinct structural motifs are observed in the structures of the predicted global minima of Au_{2-40}, based on octahedra, decahedra, icosahedra and hexagonal prisms. The octahedral clusters are $Au_{6,26,27,35,38-40}$, the decahedral clusters are $Au_{15-19,29,31,37}$, the icosahedral clusters are $Au_{12,13,23,28,33,34,36}$ and the hexagonal prismatic structures are $Au_{14,20,21,24}$. Other nuclearities have low-symmetry global minima which do not conform to these structural motifs and which have been termed "amorphous".

The 12 atom cluster forms an uncentred icosahedron rather than the more usual icosahedron with a vertex missing. The 13 atom icosahedron and 38 atom truncated octahedron are predicted as global minima, but the 19 atom cluster is a decahedral cluster rather than the more commonly observed double icosahedron.

Much of the structural data on gold clusters is for clusters with their surfaces passivated by surfactant ligands such as organic thiols [3–7]. In the future we will extend this study to include the effects of thiolate ligands on the structures and stabilities of gold clusters.

The coordinate files for all the minima found in this study and other ancillary information are available at the Birmingham Cluster Web site [39].

The authors would like to thank Dr. H. Cox for deriving the potential used in this study and for many useful discussions. NTW would also like to thank EPSRC for the award of a Ph.D. studentship.

References

1. *Clusters of atoms and molecules*, edited by H. Haberland (Springer, Berlin, 1994).
2. R.L. Johnston, Phil. Trans. Roy. Soc. Lond. A **356**, 211 (1998).
3. R.L. Whetten, J.T. Khoury, M.M. Alvarez, S. Murthy, I. Vezmar, Z.L. Wang, P.W. Stephens, C.L. Cleveland, W.D. Luedtke, U. Landman, Adv. Mater. **8**, 428 (1996).
4. M.M. Alvarez, J.T. Khoury, T.G. Schaaff, W. Shafigullin, I. Vezmar, R.L. Whetten, Chem. Phys. Lett. **266**, 91 (1997).
5. C.L. Cleveland, U. Landman, M.N. Shafigullin, P.W. Stephens, R.L. Whetten, Z. Phys. D **40**, 503 (1997).
6. C.L. Cleveland, U. Landman, T.G. Schaaff, M.N. Shafigullin, P.W. Stephens, R.L. Whetten, Phys. Rev. Lett. **79**, 1873 (1997).
7. T.G. Schaaff, M.N. Shafigullin, J.T. Khoury, I. Vezmar, R.L. Whetten, W.G. Cullen, P.N. First, C. Gutiérrez-Wing, M.J. Ascensio, M.J. Jose-Yacamán, J. Phys. Chem. B **101**, 7885 (1997).
8. J.N. Murrell, R.E. Mottram, Mol. Phys. **69**, 571 (1990).
9. H. Cox, R.L. Johnston, J.N. Murrell, J. Sol. State Chem. **145**, 517 (1999) and reference therein.
10. H. Cox, X.H. Liu, J.N. Murrell, Mol. Phys. **93**, 921 (1998).
11. J. Uppenbrink, R.L. Johnston, J.N. Murrell, Surf. Sci. **304**, 223 (1994).
12. J.Y. Fang, R.L. Johnston, J.N. Murrell, Mol. Phys. **78**, 1045 (1993).
13. W.A. de Heer, Rev. Mod. Phys. **65**, 611 (1993).
14. M.P. Allen, D.J. Tidesley, *Computer Simulation of Liquids* (Oxford Science Publications, 1987).
15. A.R. Leach, *Molecular Modelling, Principles and Applications* (Longman, 1996).
16. N.T. Wilson, R.L. Johnston, *CLUSPRO97*, University of Birmingham, 1997.
17. W.H. Press, S.A. Teukolsky, W.T. Vetterling, B.P. Flannery, *Numerical Recipes in Fortran 77: The Art of Scientific Computing* (Cambridge University Press, second edition, 1996).
18. C. Zhu, R.H. Byrd, P. Lu, J. Nocedal, Northwestern University EECS Technical Report NAM12, 1995.
19. J.A. Northby, J. Xie, D.L. Freeman, J.D. Doll, Z. Phys. D **12**, 69 (1989).
20. J.W. Lee, G.D. Stein, J. Phys. Chem. **91**, 2450 (1987).

21. D.J. Wales, J.P.K. Doye, J. Phys. Chem. A **101**, 5111 (1997).
22. H. Partridge, C.W. Bauschlicher, S.R. Langhoff, Chem. Phys. Lett. **175**, 531 (1990).
23. R.B. Ross, W.C. Ermler, J. Phys. Chem. **89**, 5202 (1985).
24. J.M. Seminario, J.M. Tour, Int. J. Quant. Chem. **65**, 749 (1997).
25. O.D. Häberlen, S.C. Chung, M. Stener, N. Rösch, J. Chem. Phys. **106**, 5189 (1997).
26. J.P.K. Doye, D.J. Wales, New J. Chem. **22**, 733 (1998).
27. J.E. Hearn, R.L. Johnston, J. Chem. Phys. **107**, 4674 (1997).
28. L.D. Lloyd, R.L. Johnston, Chem. Phys. **236**, 107 (1998).
29. L.D. Lloyd, R.L. Johnston, J. Chem. Soc., Dalton Trans., 307 (2000).
30. J.P.K. Doye, D.J. Wales, J. Chem. Soc., Farad. Trans. **93**, 4233 (1997).
31. D.J. Wales, J.P.K. Doye, A. Dullweber, F.Y. Naumkin, The Cambridge Cluster Database, URL `http://www.brian.ch.cam.ac.uk/CCD.html`.
32. I.L. Garzòn, J. Jellinek, Z. Phys. D **20**, 235 (1991).
33. I.L. Garzòn, J. Jellinek, Z. Phys. D **26**, 316 (1993).
34. I.L. Garzòn, K. Michaelian, M.R. Beltràn, A. Posada-Amarillas, P. Ordejòn, E. Artacho, D. Sànchez-Portal, J.M. Soler, Phys. Rev. Lett. **81**, 1600 (1998).
35. I.L. Garzòn, A. Posada-Amarillas, Phys. Rev. B **54**, 11796 (1996).
36. K. Michaelian, N. Rendon, I.L. Garzòn, Phys. Rev. B **60**, 2000 (1999).
37. S. Sawada, S. Sugano, Z. Phys. D **20**, 259 (1991).
38. F. Ercolessi, W. Andreoni, E. Tosatti, Phys. Rev. Lett. **66**, 911 (1991).
39. R.L. Johnston, N.T. Wilson, Birmingham Cluster Web, URL `http://www.tc.bham.ac.uk/bcweb`.